scientific reports

Check for updates

OPEN

Protamine labeling with Reactive Black-5 and its molecularly designed derivatives visualize vacuoles in human sperm head

Satoru Kaneko[1,2]✉, Yukako Kuroda[3,4], Ami N. Saito[5], Moriaki Sakihara[5], Kazuya Inagaki[5], Junichiro Yamaguchi[5] & Yuki Okada[1]

To date, numerous studies have examined the etiological relationship between vacuoles and DNA fragmentation in human sperm, with vacuoles typically assessed using differential interference contrast microscopy. To explore the optimal dye for visualizing vacuoles, we collected 12 commercially available reactive dyes and compared their staining performance. Labeling protamines with 9.0 µmol/L Reactive Black-5 (RB5) stained the nuclear body bluish and visualized vacuoles as unstained spots. Next, we synthesized 30 molecularly designed RB5 derivatives to identify an optimal molecular structure for vacuole observation, guided by structure–activity relationship analyses. Introducing 2-methylbenzenesulfonate into 4-amino-5-hydroxy-2,7-naphthalenedisulfonic acid (compound 2221) provided the minimal π-conjugation needed to produce a blue color. At 1.0 µmol/L, 2221 showed staining performance comparable to that of 9.0 µmol/L RB5. Both dyes visualized not only large vacuoles but also small sporadic vacuoles. Dissociation of the DNA–protamine complex with sodium dodecyl sulfate, reduction of disulfide bonds with dithiothreitol, and re-crosslinking of protamines with RB 5 transformed the outlines into an oval shape. RB5 staining gave enough contrast between the nuclear body and the vacuoles for quantitative morphometric analyses.

Keywords Human sperm, Vacuole, Reactive black 5, Structure–activity relationship analysis, Molecular design, Oval head

The term "semen quality" has been used as a surrogate parameter for human male fecundity. Observation of sperm concentration, motility, and head morphology under a phase-contrast microscope has been recognized as the primary means of examining male infertility. The WHO recommends deep staining with Papanicolaou or rapid May–Giemsa staining to observe the sperm morphology[1], with normality diagnosed according to the strict criteria established by Kruger et al.[2].

While investigating the pharmacological actions of antagonists for ATP-activated channels in human sperm, we serendipitously discovered that Reactive Blue-2 (RB2), a highly potent P2Y purine-receptor antagonist[3], weakly stained the head a translucent blue and visualized vacuoles as toneless spots[4]. RB2 stained the heads of human sperm and the nuclei of human lymphocytes at neutral pH, whereas it selectively stained sperm at pH 10[4,5]. Approximately 20–30% of amino acids in histones consist of lysine (Lys) and arginine (Arg), whereas 60–70% of amino acids in protamines consist of Arg[6]. The dissociation constants (pk3) for the amino residue in Lys and the guanidyl residue in Arg are 10.5 and 12.5, respectively. Three sulfonate residues in RB2 bound electrostatically with Arg, but not with Lys at pH 10. This pH-dependent cellular specificity was due to differences in Arg content between protamines and histones[5]. RB2 revealed that the features of vacuoles were heterogeneous both inter-individually and inter-sperm within an ejaculate[4,5]. Fluorescent staining with SYBR Gold also visualized vacuoles as low-density areas of DNA[4]. After protamination, intra- and inter-cross-linkages of cysteine in protamines condense and arrange the sperm head[7]. RB2 visualized degraded spermatids that had undergone protamination but were arrested prior to tail elongation[5], revealing that the majority of semen

[1]Laboratory of Pathology and Development, Institute for Quantitative Biosciences, The University of Tokyo, 1-1-1 Yayoi, Bunkyo, Tokyo 113-0032, Japan. [2]Sperm-Semen-Epididymis-Testis (SSET) Clinic, 1-5 Kanda-Iwamoto, Chiyoda, Tokyo 101-0033, Japan. [3]Department of Obstetrics and Gynecology, Fukushima Medical University, Hikarigaoka, Fukushima, Fukushima 960-1295, Japan. [4]KURODA International Medical Reproduction, 2-22-1 Shinkawa, Chuo, Tokyo 104-0033, Japan. [5]Department of Applied Chemistry, Waseda University, 513 Wasedatsurumakicho, Shinjuku, Tokyo 162-0041, Japan. ✉email: kanekosatoru@iqb.u-tokyo.ac.jp

specimens diagnosed to be azoospermia under phase contrast microscopy contained a small number of sperm as well as spermatids in various phases[5].

Labeling protamines with specific reactive dyes is a powerful tool for investigating human sperm function and spermiogenesis. The vacuoles recorded in photographs must be digitized for quantitative analysis. Although the light-blue coloring with RB2 provides sufficient contrast for visual observation[4,5], it is too insufficient for gradient processing.

Some dyes are usually synthesized via condensation reactions of various small organic fragments, producing characteristic chromophores. Their intermolecular forces, such as van der Waals, hydrophobic, hydrogen, electrostatic forces, and covalent bonds, generate characteristic adsorption to cellular components. In the present study, we collected 12 commercially available reactive dyes containing more than one sulfonate residue and compared their dyeing characteristics with those of RB2. Notably, Reactive Black-5 (RB5) exhibited satisfactory dyeing characteristics, particularly its deep-blue coloring, which was preferable for both visual observation and digital processing. We synthesized 30 molecularly designed derivatives of RB5 to explore optimal molecular structures through structure–activity relationship analyses. RB5 staining gave enough contrast between the nuclear body and the vacuoles for quantitative morphometric analyses.

Results

Histological staining often uses high concentration dye to enhance contrast, and high-contrast images are preferable for binary image processing. Even after separating the motile sperm, the features of vacuoles in the resulting fraction differed among individuals. All reactive dyes examined in the present study stained the heads; however, increasing dye concentration obscured the vacuoles, particularly small, sporadic vacuoles. Our previous studies examined the minimal dye concentration needed to distinguish them from the nuclear body. We selected a specimen with small sporadic vacuoles and determined the optimal dye concentration to maximize their contrast. Qualitatively, blue dyes provided better contrast than red dyes. Figures 1 and 2 illustrate the structural formulas and staining profiles of RB2, RB5, RB171, and RB222. When comparing two blue-dye scaffolds, AHNS derivatives provided greater contrast than anthraquinone derivatives such as RB2. Although the pale-blue coloring with 0.4 mmol/L RB2 produced sufficient contrast for visual inspection (Fig. 2A), highly diluted RB5 (9.0 µmol/L), textile-grade RB171 (0.001%), and RB222 (0.0005%) yielded excellent contrast for both visual inspection and image processing (Fig. 2B–D). Notably, the RB5 solution was nearly transparent yet revealed small sporadic vacuoles with stark contrast.

Commercially available reactive dyes are often structurally complex (Fig. 1). The simple, symmetric structure of RB5 facilitates analysis of the structure–activity relationship. We synthesized 30 derivatives to optimize the side-chain structure of AHNS. Figure 3 shows the structural formulas and staining profiles of AHNS, its derivatives, and methyl green (MG). Figure 4 shows the characteristic derivatives used to guide our analysis. As is well known, the chromophore of organic dyes typically depends on delocalization of π electrons in a π-conjugated system[8]. Although the aqueous solution of 30 mmol/L AHNS exhibited a dark-blown color, it barely colored the head, attaching one (compound 2201) or two (2266) benzene rings through azo bonding with AHNS, thereby satisfying the minimum π conjugation required for color development. Their aqueous solutions (30 mmol/L) appeared purple and dark blue, respectively. As mentioned earlier, we focused on the blue color derivatives. Various organic components were further attached to 2266; 2221, 2163, and 2228 were noteworthy to understand the structure–activity relationship (Fig. 4). Although the dyeing power was significantly inferior to

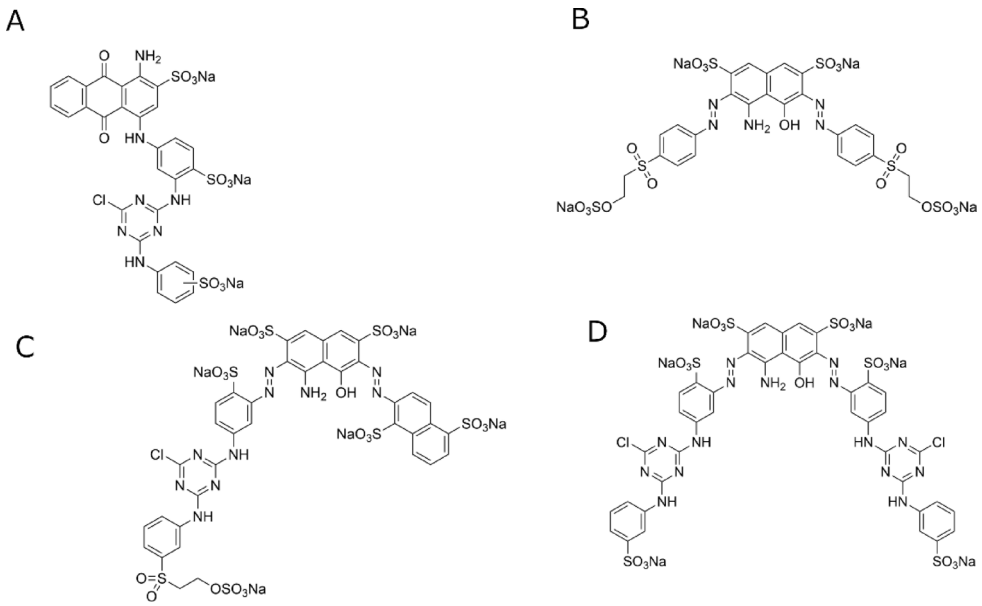

Fig. 1. Structural formula of selected commercially supplied reactive dyes. (**A**) Reactive Blue 2, (**B**) Reactive Black 5, (**C**) Reactive Blue 222, (**D**) Reactive Blue 171.

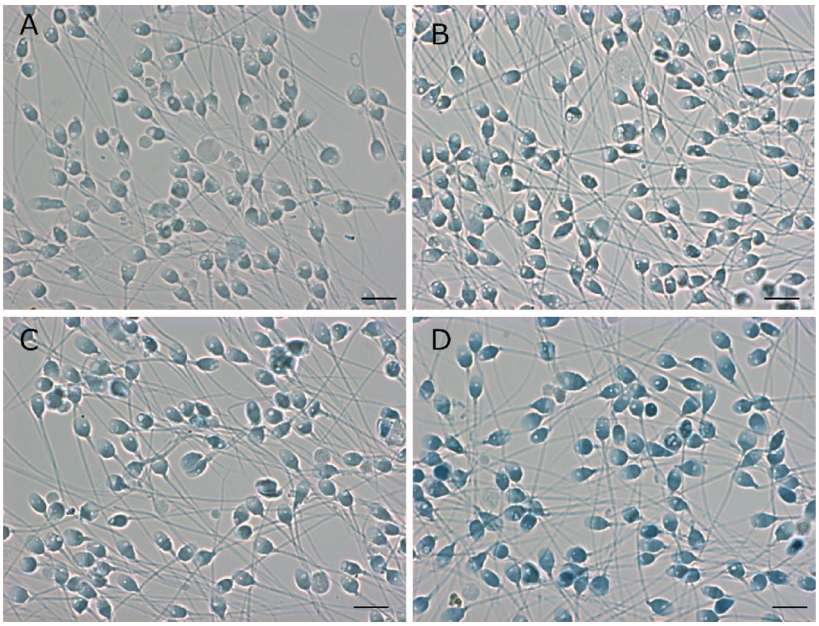

Fig. 2. Dyeing performance and molecular characteristics of the reactive dyes. The motile sperm fraction (volume: 0.5 mL, sperm concentration: 25×10^6/mL, motility: 90%), which displayed small sporadic vacuoles, was prepared from a semen specimen (3.2 mL, 90×10^6/mL, 60%). This specimen is also used in Figs. 4 and 6A,B. (**A**) 0.4 mmol/L RB2. (**B**) 9.0 µmol/L RB5. (**C**) 0.001% RB171. **D** 0.0005% RB222. The scale bars represent 10 µm.

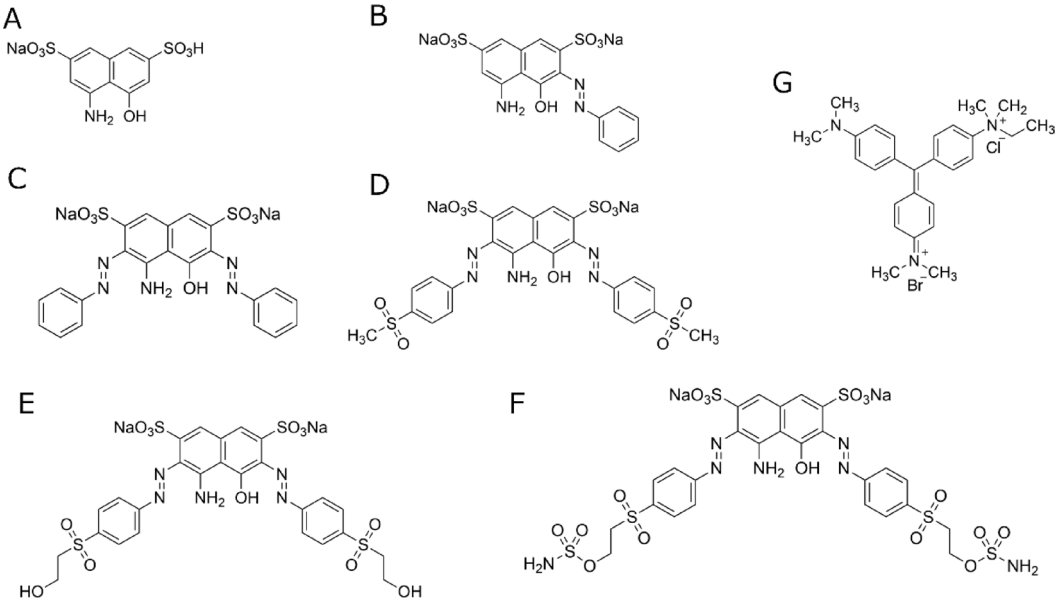

Fig. 3. Structural formulas of AHNS and selected synthetic derivatives of RB5. (**A**) AHNS, (**B**) 2201, (**C**) 2266, (**D**) 2221, (**E**) 2163, (**F**) 2228, (**G**) methyl green.

RB5 (Fig. 2B), 1.8 mmol/L 2266 imparted a bluish hue to the head (Fig. 4A). The bonding of two methylsulfonyl groups to azobenzene in 2266 (compound 2221) dramatically enhanced the dyeing power; a mere 1.0 µmol/L of 2221 provided the highest performance among 12 commercially available reactive dyes and 30 derivatives (Fig. 4B). The addition of two hydroxyethyl sulfonyl groups to 2221 is closely related to RB5. However, modifying the terminal ionic sulfonates to nonionic alcohol (2163) or sulfone amide (2228) did not result in any further enhancement of their dyeing power. Figure 4C shows the profile of 10 µmol/L 2228. We explored DNA labeling as a means to visualize vacuoles. MG, which contains two quaternary ammonium groups, is a classic basic dye

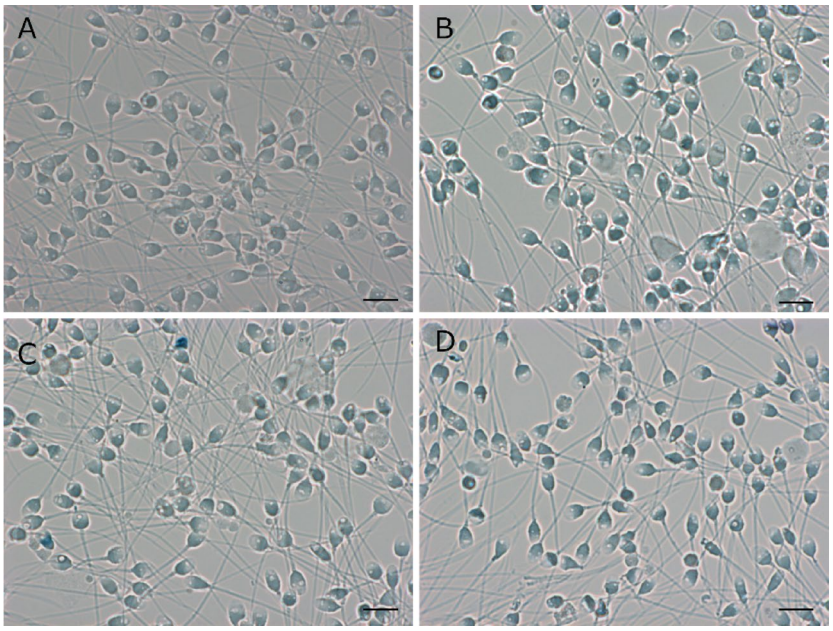

Fig. 4. Structure–activity relationship among the RB5 derivatives. (**A**) 1.8 mmol/L (2266). (**B**) 1.0 µmol/L (2221). (**C**) 10 µmol/L (2228). (**D**) 20 µmol/L methyl green (MG). The reaction between quaternary ammonium groups in MG and phosphate groups in DNA is not pH-dependent; staining was performed in 50 mmol/L HEPES–NaOH, at pH 7.4. The scale bars represent 10 µm.

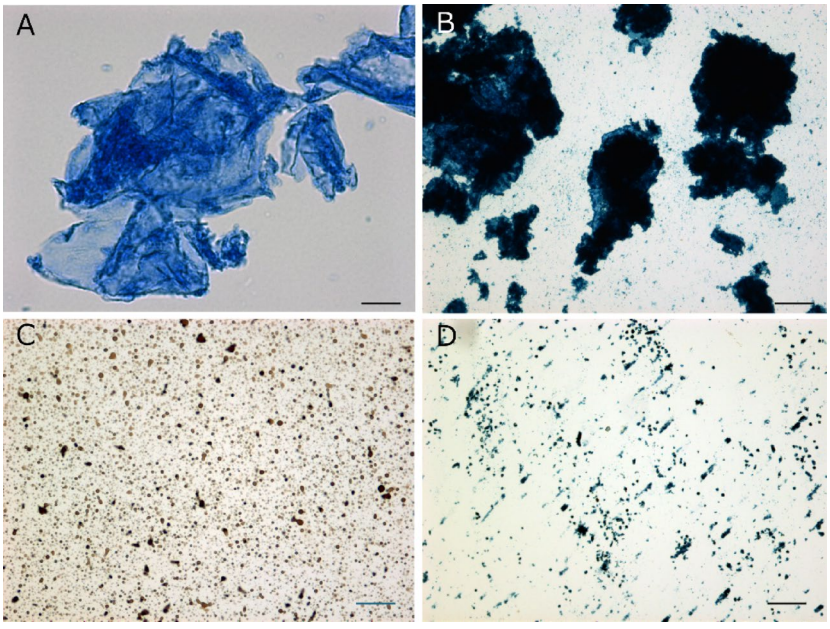

Fig. 5. Cross-linking activity of the dyes. Each dye at 3.0 mmol/L was reacted with partially purified human protamines. (**A**) Reactive Blue 2. (**B**) Reactive Blue 5. (**C**) AHNS. (**D**) 2221. The scale bar represents 50 µm.

for DNA labeling (Fig. 3). At 20 µmol/L, its staining intensity exceeded that of AHNS derivatives, including RB5; however, small vacuoles were obscured (Fig. 4D).

Figure 5 shows the cross-linking activity of the dyes as measured by the agglutination test. All commercially available reactive dyes we examined contained three or more distantly spaced ionic sulfonate groups per molecule. Figure 5A,B show RB2 and RB5, respectively; both formed cross-linked agglutinates instantaneously. In the synthesized derivatives, the sulfonate groups were converted to nonionic forms, except in AHNS. Figure 5C,D show AHNS and 2221, respectively. The activity associated with two closely positioned ionic sulfonate groups

was lower than that of RB2 and RB5: AHNS formed brown drops, and 2221 formed blue drops and rod-like agglutinates.

When dissociating the DNA protamine complex with 0.001% sodium dodecyl sulfate (SDS) and reducing disulfide bonds with 5.0 mmol/L dithiothreitol (DTT) in the presence of 9.0 µmol/L RB5, the heads became uniformly oval and swollen, facilitating RB5 permeation into the nucleus; staining was deeper and caused disappearance of vacuoles (Fig. 6A). Ionized sulfonate in SDS and RB5 competitively dissociated DNA protamine complex, 4 sulfonates in RB5 simultaneously re-cross-linked guanidyl groups in the depolymerized protamines electrostatically. The size of the swollen oval was determined by the molar ratio of SDS and RB5. Figure 6A,D show the optimal ratio for forming a smooth oval with a sharp edge. In the absence of RB5, SDS with mono sulfonate formed a spongy ghost (Fig. 6B). As the concentration of SDS increased, it was finally dispersed. In teratozoospermic semen, unseparated sperm stained with 9.0 µmol/L RB5 showed amorphous head outlines and frequent large vacuoles (Fig. 6C). After the same treatment as in Fig. 6A, the heads swelled and became oval regardless of their original outlines and caused disappearance of vacuoles (Fig. 6D).

After staining the sperm with RB5, the color photograph was converted into a binarized image (Fig. 7A). The contrast between the nuclear body and the vacuoles was sufficient for digital morphometric analysis. The same field of view was observed using DIC optics at 600× magnification; shadowing with a Nomarski prism visualized the vacuoles stereographically, while the monotonal gray image was unsuitable for binary processing (Fig. 7B). CCD digital cameras used for research mainly focus on capturing fluorescent images, often with larger pixel sizes to absorb more photon energy, resulting in fewer pixels in the sensor. All sperm images, except for Fig. 7D,G,H were taken with a 4164 × 3120-pixel CCD; these images were reduced 10 times from their original sizes (79.5 × 52.8 cm). Figure 7D shows an image captured with a 1388 × 1040-pixel CCD (original size: 23.5 × 17.6 cm), also scaled down to the same size. Figure 7E,F show the original size vacuoles from C, and G and H display the original size vacuoles from D, respectively. Since the size of a small vacuole is less than 1 µm (Fig. 7E,G), a CCD sensor with more than 4000 × 3000 pixels is essential for quantitative morphometric analysis of these vacuoles.

The sperm specimens were obtained from 13 husbands (age: 42.7 ± 8.60 years old), and the washed sperm suspensions were stained with RB5 and photographed. A total of 5,973 sperm were binarized by means of Image J (version 1.54), and the area and aspect ratio of the head and the area of the vacuole were measured. Figure 8A,B summarize the point diagrams of the aspect ratio and the occupancy rate of the largest vacuole (area of the largest vacuole/area of the head × 100). Mean ± standard deviation of these parameters were 1.59 ± 0.460 (1–6.35) and 10.2 ± 8.10% (0–47.4%), respectively (Fig. 7A). The present study tentatively defined the normal range of aspect ratio and the occupancy rate to be 1.3–1.7 and less than 10%, Fig. 8B shows the diagram of 2191 sperm including in this category with mean of 1.50 ± 0.163 and 4.90 ± 2.87%, the sperm looked like evenly distributed and there was no convergent point. Figure 8C,D summarize the mean ± standard deviation of the aspect ratio and the occupancy rate in each specimen. Human sperm heads typically range from 4.0 to 5.5 µm in length and

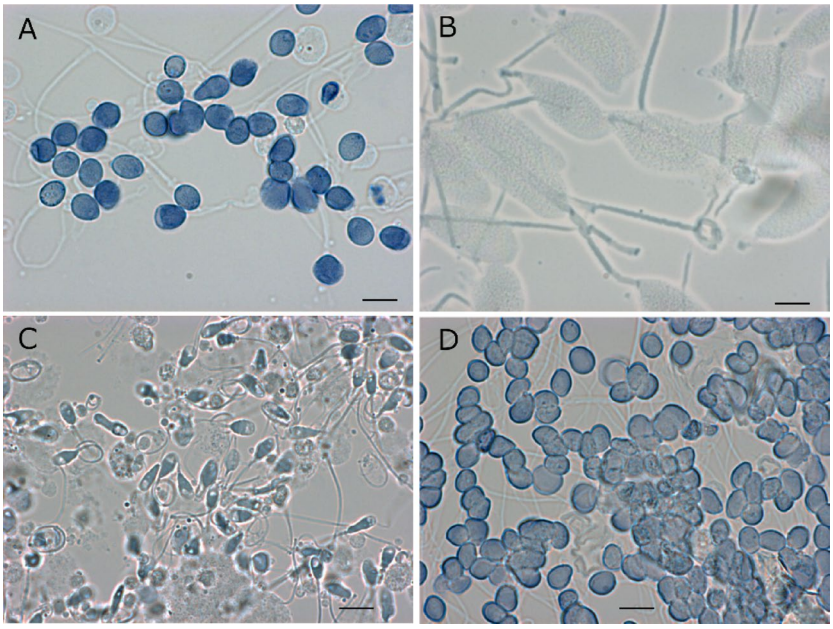

Fig. 6. Effect of dissociation of DNA-protamine complex and reduction of disulfide bonds on the dyeing characteristics of RB5. (**A**) The sperm specimen corresponding to Fig. 2B was stained with 9.0 µmol/L RB5 in the presence of 0.001% SDS, 5 mmol/L DTT, 0.1 mol/L Na_2CO_3–$NaHCO_3$, pH 10.0 for 10 min. (**B**) The sperm was treated in the same manner as A without RB5. (**C**) Teratozoospermic semen (2.2 mL, 30×10^6/mL, 30%) was diluted 10 times with saline and centrifuged in a swing-out rotor at 400×*g* for 10 min. The sediment was designated as the unseparated sperm. D: The sperm in C was treated in the same manner as A. The scale bar represents 10 µm.

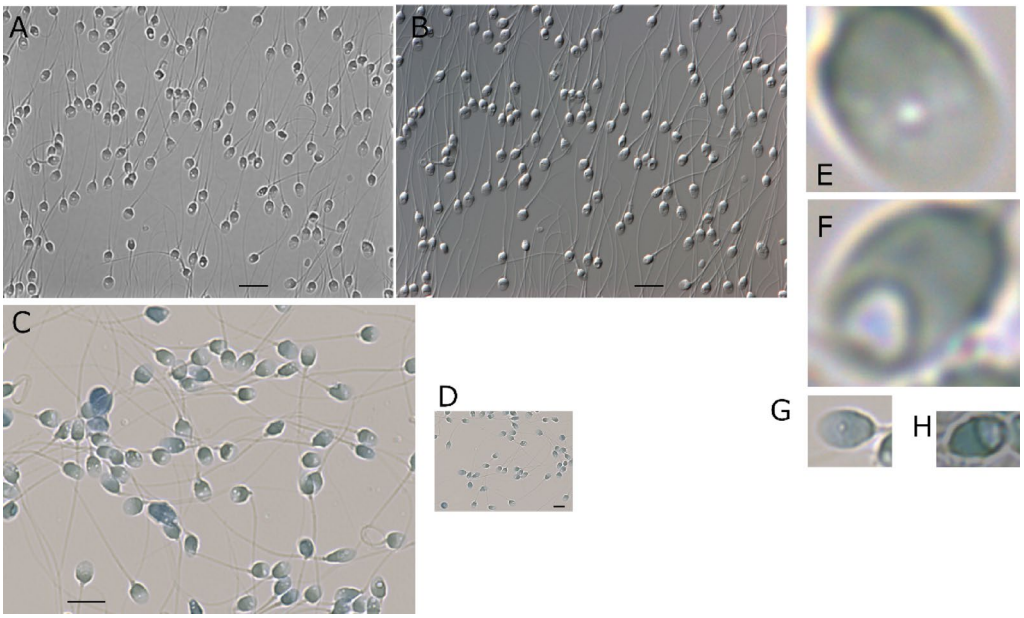

Fig. 7. Technical requirements for morphometric analysis—DIC optics and resolution of CCD sensor. The motile sperm fraction (volume: 0.1 mL, sperm concentration: 34×10^6/mL, motility: 90%) was prepared from a semen specimen (2.8 mL, 42×10^6/mL, 50%). Photographs A and B were taken with the same field of view: bright-field optics after staining with RB5 and DIC optics at 600 magnification, respectively. After staining the sperm with RB5, the photographs were taken with a 4164 × 3120-pixel CCD (**C**) or with a 1388 × 1040-pixel CCD (**D**). The scale bar represents 10 μm.

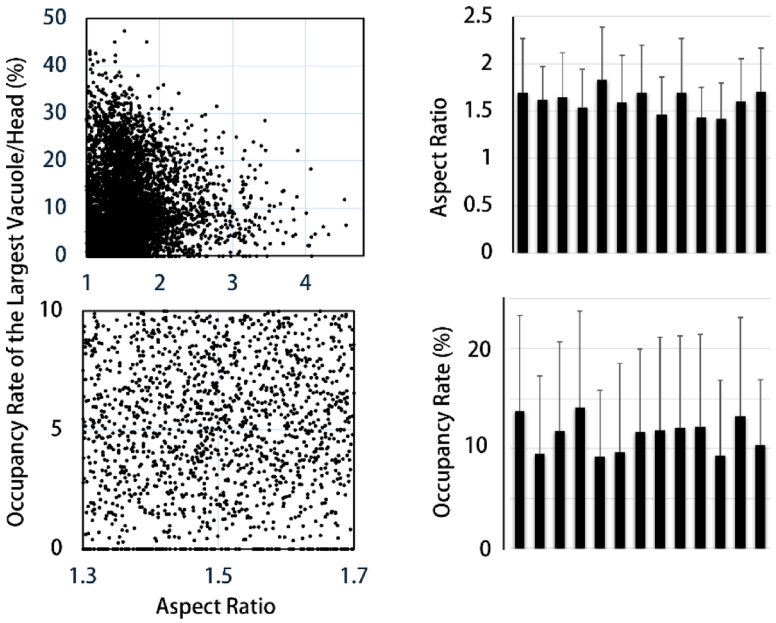

Fig. 8. Point diagrams of the aspect ratio and the occupancy rate of the largest vacuole in the head. Thirteen semen specimens (volume: 3.27 ± 1.14 mL, sperm concentration: $25.0 \pm 13.4 \times 10^6$/mL, motility: 40.0 ± 17.3%) were obtained from the husbands (age: 42.7 ± 8.60 years old). After separating motile sperm, the washed sperm suspension (volume: 0.1 mL; sperm concentration: $29.8 \pm 19.8 \times 10^6$/mL; motility: 60.7 ± 7.80%) was stained with RB5 and photographed using a 4164 3120-pixel CCD. (**A**) Point diagram of a total of 5973 sperm examined. (**B**) Point diagram of 2191 sperm, including the range of aspect ratio and the occupancy rate in 1.3–1.7 and less than 10%. The bar graphs show the mean ± standard deviation of the aspect ratio (**C**) and the occupancy rate (**D**) in each specimen.

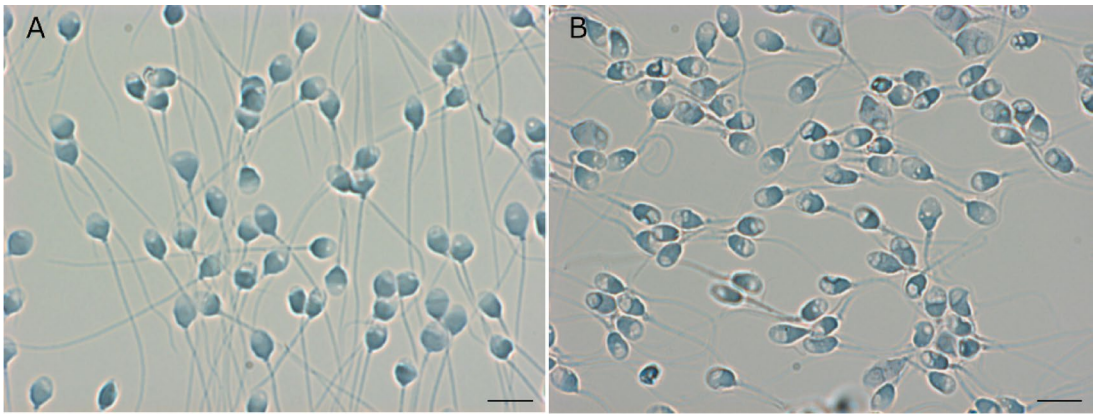

Fig. 9. Two notable vacuolar features in the separated motile sperm fractions. (**A**) The motile sperm fraction (0.5 mL, 35×10^6/mL, 90%) was prepared from a semen specimen (5.2 mL, 80×10^6/mL, 60%). (**B**) The motile sperm fraction (volume: 0.5 mL, sperm concentration: 20×10^6/mL, 90%) was prepared from a semen specimen (4.6 mL, 35×10^6/mL, 40%). **E** and **F** show the original-sized vacuoles in **C**, while **G** and **H** also display the original-sized vacuoles in **D**. The scale bar represents 10 µm.

2.5 to 3.5 µm in width[9], corresponding to the aspect ratio of 1.14–2.20. In the present study, 91.5% of sperm (5466) were 1 or 2, with a mean of 1.6. Figures 2, 6C, 7A,C and 8D suggested that not only the size of the largest vacuole but also the number and size of vacuoles were diverse among inter-sperm and inter-individuals. The occupancy rate of 4120 sperm (69.2%) was less than 30%. Only 203 sperm (3.4%) were free from the vacuole.

Figure 9 demonstrates two notable sperm fractions: in both, head outlines were smooth oval and motility exceeded 90%, but their vacuolar features differed markedly. In Fig. 9A, almost all sperm had no vacuole or only a small vacuole; this case was exception rather than a rule. Figure 9B was also very rare: almost all sperm contained large vacuoles in the anterior portion of the head. It remains unclear why a particular vacuole form occurred at a particular location without accompanying deformation of the outline.

Discussion

Reactive dyes are among the most widely used and important dyes in the textile industry[10,11]. Their structures typically comprise one or two core scaffolds with various side chains, including reactive groups such as 1,3,5-triazine chloride, vinyl sulfone, and benzene sulfone. These dyes form covalent bonds with cellulose, wool, and nylon, conferring good fastness to textiles[10,11]. RB2, a family of the reactive dye, is well known as a ligand for group-specific dye affinity chromatography[12] of certain dehydrogenases that require NAD as a coenzyme[13], as well as albumin[14] and interferon[15]. Because highly diluted RB2 provides contrast for vacuoles within the nuclear body (Fig. 2A), the present study explores some alternatives to RB2.

The cross-comparison of commercially available dyes and newly synthesized RB5 derivatives revealed the following structure–activity relationship: although AHNS was ineffective as a dye, the attachment of two azobenzene groups provided the minimum π-conjugation required to produce color in 2266. However, the dyeing power of 2266 was significantly inferior to that of the commercially available dyes, as shown in Fig. 2. The addition of two methylsulfonyl groups to 2266 significantly enhanced the dyeing power, with 1.0 µmol/L of 2221 demonstrating the highest dyeing performance among those tested in the present study. However, further bonding of the de-ionized hydroxyethyl sulfonyl group to 2221 did not yield any additional enhancement in dyeing power.

In contrast to textile dyeing, ionic sulfonates are unlikely to form covalent bonds with cellular components; instead, they participate in electrostatic interactions. We hypothesized that multiple-point adsorption of dyes to nuclei would enhance dyeing performance. The close positioning of the two ionic sulfonates in 2221 provides sufficient binding affinity to protamines, effectively coloring the head (Fig. 4B). The addition of two ionic sulfonyl groups at the tips of the side chains in RB5 further enhanced cross-linking activity (Fig. 5B).

Commercially supplied reactive dyes usually include several reactive groups for textile dyeing. Comparison of the formulas of RB5 and RB171 (Fig. 1) suggests that the triazine ring, a reactive group for cellulose, is not essential for binding to nuclei. The simple structure of 2221 further suggests that the triazine ring and the ionic benzenesulfonate and vinylsulfonate groups are not essential for interaction with nuclei or for dyeing performance. From another perspective, a reduced number of ionic sulfonates in a molecule causes poor water solubility. Structurally, 2221 is no longer classified as a reactive dye.

Figure 4D suggests that labeling of either protamines or DNA could visualize vacuoles. The quaternary ammonium groups in MG interact nonspecifically with anionic molecules over a wide pH range and stain debris in unseparated semen samples. We therefore abandoned plans to visualize vacuoles via DNA labeling. In the interim, we recommend commercially available, inexpensive, reagent-grade RB5 as a dye for visualizing vacuoles, and we expect further improvement of 2221.

Several studies have described motile sperm organelle morphology examination (MSOME), which uses an additional 6× digital zoom on high-magnification DIC images (1000×)[16–18]. Because vacuoles are believed to

impair DNA stability, intraoperative selection by MSOME to exclude vacuolated sperm has been reported to enhance embryo development to the blastocyst stage[16–18]. However, no consensus has been reached, mainly due to technical limitations of the analytical methods. Digital morphometric assessment of the size, number, location, and total area of vacuoles in separated motile sperm fractions is the initial step toward understanding this relationship. Figures 7 and 8 present our preliminary studies. Translucent RB5 staining revealed not only large vacuoles but also sporadic small vacuoles (Fig. 7A). Shadowing of the same field with the Nomarski prism visualized similar profiles stereographically (Fig. 7B). However, a monochrome image was unsuitable for binary processing. As shown in Fig. 7E, small, sporadic vacuoles were often less than 1 µm. For digital morphometric analysis, key technical requirements include use of a high-resolution CCD with over 4000 × 3000 pixels and non-use of a 6× digital zoom, which simply enlarges pixel size and reduces image resolution.

Cancelling of electrostatic repelling by bonding of protamines to DNA, followed by intra- and intermolecular cross-linking of cysteines in protamines, are major contributors to compaction of the nucleus of mature sperm[7,19]. Some articles discussed the relationship between protamine deficiency[20] and vacuole formation. Swelling the head from Figs. 2B to 6A imitated the reverse process of the compaction, and a balance between two competing forces, such as dissociation and cross-linking, was essential to form the smooth oval. This fact suggests that not only the protamine content but also deficiency and excess crosslinking may be related to vacuole formation and head rearrangement.

Morphometric analysis in Fig. 8 suggested that 91.5% of the sperm examined contained vacuoles, with the number and size of vacuoles varying among inter-sperm and interindividual comparisons. Because double-stranded breaks (DSBs) are among the most difficult DNA lesions to repair, the critical threshold of DSBs in a nucleus is extremely low[21,22]. The relationship between DSB numbers and deleterious outcomes is non-linear; once this threshold is exceeded, fertilization failure or pregnancy loss can occur. We developed angle-modulated two-dimensional single-cell pulsed-field gel electrophoresis (2D-SCPFGE) to detect early symptoms of DNA fragmentation[23,24]. Human motile sperm without DNA fragmentation and immotile sperm at the end stage of fragmentation were prepared for use as negative and positive standards using the same protocol as in the present study[23,24]. In our preliminary observations, the negative standards often included sperm with vacuoles; the profile shown in Fig. 9A was rather rare. The vacuoles may not be directly responsible for DNA fragmentation; we cannot dismiss the possibility of physiologic and pathologic vacuoles. The next step is to determine their thresholds using morphometric analyses.

The current translucent staining method challenges traditional histological staining, which intensively dyes tissues to enhance contrast. Since the vacuoles were concealed at higher concentrations, RB5 was highly diluted to produce minimal contrast. Now, we further modify the structure of 2221 to enhance the molecular extinction coefficient and improve the accuracy of binary processing.

Methods

Ethics statement

Human semen specimens were obtained from husbands who visited SSET clinic, Tokyo, for semen analyses. The aim of this study and the measurement items were clearly explained to the patient couples. Since the specimens were emitted from the body by masturbation, the couples understood that there was no hazard or risk to the husband, and they accepted using the residual portion of the specimens in this study. All patient couples provided written informed consent for inclusion in the manuscript. All the methods in the study have been performed in accordance with the Declaration of Helsinki. The ethical committee of the SSET clinic specifically approved this study (approval number: S24-02).

Sperm concentration and motility were measured according to methods specified in the WHO reference manual[25]. Motile human sperm were purified as previously described[23,24,26,27]. Briefly, normozoospermic semen was processed by means of sedimentation equilibrium in isotonic OptiPrep (apparent density 1.17 g/mL; Axis Shield, San Jose, CA, USA). Following ultracentrifugation at 10,000×*g* for 10 min, sperm at the interface were collected and further separated by differential-velocity sedimentation in isotonic 90% Percoll (apparent density 1.12 g/mL). After centrifugation at 400×*g* for 30 min, motile sperm were recovered from the sediment.

We examined 12 commercially supplied reactive dyes. RB2 (3/0, x/y values denote the numbers of ionic and nonionic sulfone groups), Reactive Blue-3 (2/0), and Reactive Blue-5 (4/0) share 9,10-dioxo-9,10-dihydroanthracene as the parent scaffold. Reactive Blue-13 (3/0), Reactive Blue-160 (5/0), Reactive Blue-171 (6/0), Reactive Blue-222 (6/1), Reactive Red-120 (6/0), Reactive Red-141 (8/0), Reactive Red-145 (4/1), Reactive Red-195 (5/1), Reactive Red-250 (4/1), and Reactive Black-5 (4/0; RB5) share 4-amino-5-hydroxy-2,7-naphthalenedisulfonic acid (AHNS).

Of these, the detailed information was available for three dyes; pharmacological grade RB2 (molecular weight: 774, nominal purity: more than 99%, Alexis Biochemicals, CA, USA), reagent grade RB5 (molecular weight: 951, purity: more than 85%, Tokyo Chemical Industries, Tokyo, Japan), and reagent grade AHNS (molecular weight: 341, purity: more than 80%, Tokyo Chemical Industries, Tokyo, Japan). The remaining dyes were of industrial textile grade. Thirty analogs of RB5 were synthesized by attaching various side chains to AHNS through azo bonding. Their purities were analyzed using high-throughput liquid chromatography; all products showed purities over 99.9%. This study reported concentrations of textile- and reagent-grade dyes as percentages and as moles per liter, respectively.

Staining intensity varied among dyes. Each dye was dissolved in 0.1 mol/L Na_2CO_3–$NaHCO_3$ buffer, pH 10.0, to achieve appropriate staining under a bright-field transmitted-light upright microscope (Axio Imager A1; Carl Zeiss MicroImaging, Jena, Germany), unless otherwise mentioned, images were taken at 1000× oil immersion. The images in Fig. 8A and B were taken with a 60× objective lens with or without a Nomarski prism.

Purified or unseparated human sperm were adhered to glass slides by a centrifugal autosmear method, fixed with methanol, incubated with 0.3 mL dye for 10 min, and then rinsed with tap water to remove excess dye. Still

images were recorded using a high- and low-resolution, charge-coupled device camera (AxioCam HRC; Carl Zeiss MicroImaging, Jena, Germany; 4164 × 3120 pixels and 1388 × 1040 pixels). Unless otherwise mentioned, images were taken with high-resolution mode.

Partially purified human protamines were prepared according to the previous reports[24,28]. Briefly, motile sperm were suspended in a cell lysis medium (0.1 mol/L Na_2CO_3–$NaHCO_3$, 2.0 mol/L guanidine sulfate, 5.0 mmol/L dithiothreitol (DTT), pH 10.0). DNA dissociated from protamines was gelatinized and then shrunk with benzalkonium chloride. Protamines in the supernatant were recovered by ethanol precipitation and then resolved in 1.0 mL of 0.1 mol/L Na_2CO_3–$NaHCO_3$, pH 10.0.

The cross-linking activity of the dyes with the protamines was observed using an agglutination test. Each 10 µL of some dye (0.1 mol/L Na_2CO_3–$NaHCO_3$, pH 10) was mixed with partially purified human protamines on a glass slide. The dyes immediately formed a colored agglutinate by cross-linking the protamines.

Data availability

The datasets generated and analyzed in the present study including raw images are available from the corresponding author upon reasonable request.

Received: 16 January 2026; Accepted: 17 March 2026
Published online: 26 March 2026

References

1. WHO laboratory manual for the examination and processing of human semen, sixth edition, 55–77. (World Health Organization, 2021). Licence: CC BY-NC-SA 3.0 IGO.
2. Kruger, T. F. et al. Predictive value of abnormal sperm morphology in vitro fertilization. *Fertil. Steril.* **49**, 112–117 (1988).
3. Claes, P., van Kolen, K., Roymans, D., Blero, D. & Vissenberg, K. Reactive Blue 2 inhibition of cyclic AMP-dependent differentiation of rat C6 glioma cells by purinergic receptor-independent inactivation of phosphatidylinositol 3-kinase. *Biochem. Pharmacol.* **67**, 1489–1498 (2004).
4. Kaneko, S., Yoshida, J., Ishikawa, H. & Takamatsu, K. Low density regions of DNA in human sperm appear as vacuoles after translucent staining with reactive blue 2. *J. Med. Diagn. Methods* **2**, 145. https://doi.org/10.4172/2168-9784.1000145 (2013).
5. Kaneko, S., Okada, Y., Yokota, S. & Takamatsu, K. Reactive blue dye: Highlights of vacuoles in human sperm. *J. Med. Diagn. Methods* **12**, 400. https://doi.org/10.35248/2168-9784.23.12.400 (2023).
6. Balhorn, R. The protamine family of sperm nuclear proteins. *Genome Biol.* **8**, 227. https://doi.org/10.1186/gb-2007-8-9-227 (2007).
7. Brewer, L. R., Corzett, M. & Balhorn, R. Protamine-induced condensation and decondensation of the same DNA molecule. *Science* **286**, 120–123 (1999).
8. Schindler, F., Lupton, J. M., Feldmann, J. & Scherf, U. A universal picture of chromophores in π-conjugated polymers derived from single-molecule spectroscopy. *Proc. Natl. Acad. Sci. USA* **101**, 14695700. https://doi.org/10.1073/pnas.0403325101 (2004).
9. Giuseppe Bellastella, G. et al. Dimensions of human ejaculated spermatozoa in Papanicolaou-stained seminal and swim-up smears obtained from the Integrated Semen Analysis System. *Asian J. Androl.* **12**(6), 871–879 (2010).
10. Lewis, D. M. The chemistry of reactive dyes and their application processes. In *Handbook of Textile and Industrial Dyeing, Vol 1. Principles, Processes and Types of Dyes* (ed. Clark, M.) 303–364 (Woodhead Publishing, 2011).
11. Tappe, H., et al. Reactive dyes. In *Ullmann's Encyclopedia of Industrial Chemistry*. (Wiley-VCH, 2000). https://doi.org/10.1002/14356007.a22_651
12. Lowe, C. R. & Pearson, J. C. Affinity chromatography on immobilized dyes. *Methods. Enzymol.* **104**, 97–113 (1984).
13. Labrou, N. E. & Clonis, Y. D. Biomimetic dye affinity chromatography for the purification of bovine heart lactate dehydrogenase. *J. Chromatogr. A* **718**, 35–44 (1995).
14. Leatherbarrow, R. J. & Dean, P. D. Studies on the mechanism of binding of serum albumins to immobilized Cibacron Blue F3G A. *Biochem. J.* **189**, 27–34 (1980).
15. Knight, E. Jr. & Fahey, D. Human fibroblast interferon. An improved purification. *J. Biol. Chem.* **256**, 3609–3611 (1981).
16. Bartoov, B. et al. Pregnancy rate are higher with intracytoplasmic morphologically selected sperm injection than with conventional intracytoplasmic injection. *Fertil. Steril.* **80**, 1413–1419 (2003).
17. Vanderzwalmen, P. et al. Blastocyst development after sperm selection at high magnification is associated with size and number of nuclear vacuoles. *Reprod. Biomed. Online* **17**, 617–627. https://doi.org/10.1016/S1472-6483(10)60308-2 (2008).
18. Berkovitz, A. et al. Does the presence of nuclear vacuoles in human sperm selected for ICSI affect pregnancy outcome?. *Hum. Reprod.* **21**, 1787–1790. https://doi.org/10.1093/humrep/del049 (2006).
19. Okada, Y. Sperm chromatin condensation: Epigenetic mechanisms to compact the genome and spatiotemporal regulation from inside and outside the nucleus. *Genes. Genet. Syst.* **97**, 41–53 (2022).
20. Ni, K., Spiess, A. N., Schuppe, H. C. & Steger, K. The impact of sperm protamine deficiency and sperm DNA damage on human male fertility: A systematic review and meta-analysis. *Andrology* **4**, 789–799 (2016).
21. van Gent, D. C., Hoeijmakers, J. H. & Kanaar, R. Chromosomal stability and the DNA double-stranded break connection. *Nat. Rev. Genet.* **2**, 196–206 (2001).
22. Ceccaldi, R., Rondinelli, B. & D'Andrea, A. D. Repair pathway choices and consequences at the double-strand break. *Trends Cell Biol.* **26**, 52–64 (2016).
23. Kaneko, S. & Okada, Y. Revalidation of DNA fragmentation analyses for human sperm—Measurement principles, comparative standards, calibration curve, required sensitivity, and eligibility criteria for test sperm. *Biology* **13**, 484 (2024).
24. Kaneko, S. & Takamatsu, K. Angle modulated two-dimensional single cell pulsed-field gel electrophoresis for detecting early symptoms of DNA fragmentation in human sperm nuclei. *Sci. Rep.* **14**, 840 (2024).
25. WHO laboratory manual for the examination and processing of human semen, sixth edition, 29–39. (World Health Organization, 2021). Licence: CC BY-NC-SA 3.0 IGO.
26. Kaneko, S. & Takamatsu, K. Re-evaluation of significance of anti-sperm antibodies in clinical immune infertility-antigenicity of human sperm diminishes during DNA fragmentation. *J. Med. Diagn. Methods* **12**, 439. https://doi.org/10.35248/2168-9784.23.12.440 (2023).
27. Kaneko, S., Okada, Y. & Takamatsu, K. Sperm specific two-step dye exclusion assays to evaluate integrity of plasma and organelle membranes—New approach for quality assurance of the sperm for intra-cytoplasmic sperm injection. *J. Med. Diagn. Methods* **12**, 450. https://doi.org/10.35248/2168-9784.23.12.450 (2024).
28. Ada Soler-Ventura, A. et al. Mammalian sperm protamine extraction and analysis, a step-by-step detailed protocol and brief review of protamine alterations. *Protein Pept. Lett.* **25**, 424–433 (2018).

Author contributions

Satoru Kaneko (S.K.), Yukako Kuroda (S.K.), Ami N., Saito (A.S.), Moriaki Sakihara (M.S.), Kazuya Inagaki (K.I.), Junichiro Yamaguchi (J.Y.), Yuki Okada (Y.O.) Conceptualization, S.K., U.K., J.Y., and Y.O.; methodology, S.K., U.K., A.S, M.S., K.I., J.Y., and Y.O.; validation, S.K., U.K., J.Y., and Y.O.; formal analysis, S.K., U.K., A.S, M.S., K.I., J.Y., and Y.O.; resources, S.K., J.Y., and Y.O.; data curation, S.K., U.K., A.S, M.S., K.I., J.Y., and Y.O.; writing-original draft preparation, S.K., U.K., J.Y., and Y.O.; writing—review and editing, S.K., U.K., J.Y., and Y.O.; visualization, S.K., U.K., A.S, M.S., K.I., J.Y., and Y.O.; supervision, S.K., and Y.O.; project administration, S.K., U.K., J.Y., and Y.O. All authors have read and agreed to the published version of the manuscript.

Funding

Translational Research Program (Grant Number A-170 and H-040) from the Japan Agency for Medical Research and Development (AMED), and the 16th GAP fund program in U-Tokyo.

Declarations

Competing interests

The authors declare no competing interests.

Additional information

Correspondence and requests for materials should be addressed to S.K.

Reprints and permissions information is available at www.nature.com/reprints.

Publisher's note Springer Nature remains neutral with regard to jurisdictional claims in published maps and institutional affiliations.